International Journal of Heat and Mass Transfer 52 (2009) 1608–1618

Contents lists available at ScienceDirect

International Journal of Heat and Mass Transfer

journal homepage: www.elsevier.com/locate/ijhmt

Analytical characterization of heat transport through biological media incorporating hyperthermia treatment

Shadi Mahjoob, Kambiz Vafai *

Mechanical Engineering Department, University of California, Riverside, CA 92521, USA

ARTICLE INFO

Article history:
Received 13 May 2008
Received in revised form 16 July 2008
Available online 1 October 2008

Keywords:
Bioheat
Porous media
Hyperthermia
Biological tissue/organ
Blood

ABSTRACT

Modeling and understanding heat transport and temperature variations within biological tissues and body organs are key issues in medical thermal therapeutic applications, such as hyperthermia cancer treatment. The biological media can be treated as a blood saturated tissue represented by a porous matrix. A comprehensive analytical investigation of bioheat transport through the tissue/organ is carried out including thermal conduction in tissue and vascular system, blood–tissue convective heat exchange, metabolic heat generation and imposed heat flux. Utilizing local thermal non-equilibrium model in porous media theory, exact solutions for blood and tissue phase temperature profiles as well as overall heat exchange correlations are established for the first time, for two primary tissue/organ models representing isolated and uniform temperature conditions, while incorporating the pertinent effective parameters, such as volume fraction of the vascular space, ratio of the blood and the tissue matrix thermal conductivities, interfacial blood–tissue heat exchange, tissue/organ depth, arterial flow rate and temperature, body core temperature, imposed hyperthermia heat flux, metabolic heat generation, and blood physical properties. A simplified solution based on the local thermal equilibrium between the tissue and the blood is also presented.

1. Introduction

Thermal transport within living organisms, bioheat transfer, is an important biological and therapeutic issue, which involves new aspects in thermal therapies, cryobiology, burn injury, disease diagnostics, and thermal comfort analysis. Thermal side effects of various treatments are important issues in bioheat investigations such as in bone drilling operation [1], frictional heating and temperature rise in total knee joint replacement [2], and in ophthalmology (laser eye surgery) [3–5]. A principal issue in medical thermal therapeutic applications, such as hyperthermia treatment, is modeling and understanding the heat transport and temperature variation within biological tissues and body organs.

Hyperthermia treatment is recognized as the fourth adjunct cancer therapy technique following surgery, chemotherapy, and radiation techniques. In hyperthermia, the tumor cells will be overheated to a therapeutic value, typically 40–45 °C to damage or kill the cancer cells and affect metastases [6,7]. Although it has been known for many years that fever can damage the cancer cells, hyperthermia technique is recently being developed as a cancer treatment by controlling and focusing the heat on the cancer cells. Hyperthermia is being utilized for many cancer types such as breast cancer, sarcomas, melanomas, bone metastases, carcinomas of the lung, stomach, pancreas, gallbladder, kidneys, neck, brain tumors, prostate tumors, and cervical cancer [8,9].

In contrast to healthy cells, a tumor is a tightly packed body of cells in which the blood circulation is restricted. Heat can cut off the oxygen and vital nutrients from the abnormal cells resulting in a breakdown in the tumor's vascular system and destruction of the cell's metabolism and subsequent devastation of tumor cells. In addition, heat causes the formation of certain proteins in the diseased cancer cells, the so-called heat shock proteins, which appear on the surface of the degenerated cells. The body immune system detects these proteins as extraneous cells, making the abnormal cells visible to the immune system.

Hyperthermia technique also improves the efficiency of other cancer therapies such as, chemotherapy and radiotherapy. Insolated cells, which would not respond to chemotherapy or radiation alone, would be subjected to heat treatment. Hyperthermia in conjunction with chemotherapy causes the drug to penetrate deeper into the tumor while augmenting the efficacy of the drug delivered to the tumor. The increased efficacy of simultaneous utilization of hyperthermia and radiotherapy or chemotherapy has been demonstrated in treatment of certain types of diseases [10], such as breast cancer [11], cervical and bladder cancer [12], rectal cancer [13], prostate cancer [14], head and neck cancer [15], superficial tumors, lung and stomach cancer and pancreas and liver metastases.

Hyperthermia treatment can be utilized either on the whole body or locally targeting the cancer cells. Whole body hyperthermia treatment is usually used for metastases, which have spread

* Corresponding author.
E-mail address: vafai@engr.ucr.edu (K. Vafai).

0017-9310/$ - see front matter © 2008 Elsevier Ltd. All rights reserved.
doi:10.1016/j.ijheatmasstransfer.2008.07.038

Nomenclature

a_{tb}	specific surface area (m^{-1})
Bi	Biot number, $h_{tb}a_{tb}D^2/k_{t,eff}$
c_p	blood specific heat ($J\,kg^{-1}\,K^{-1}$)
D	depth of the tissue/organ (m)
D_h	hydraulic diameter of the channel, $2D$ (m)
h_{tb}	blood–tissue interstitial heat transfer coefficient ($W\,m^{-2}\,K^{-1}$)
h_s	surface heat transfer coefficient for the thermal non-equilibrium model, $q_s/(T_s - T_{b,m})$($W\,m^{-2}\,K^{-1}$)
k_b	blood thermal conductivity ($W\,m^{-1}\,K^{-1}$)
$k_{b,dis}$	blood dispersion thermal conductivity ($W\,m^{-1}\,K^{-1}$)
$k_{b,eff}$	effective thermal conductivity of the blood phase ($W\,m^{-1}\,K^{-1}$)
k_t	tissue thermal conductivity ($W\,m^{-1}\,K^{-1}$)
$k_{t,eff}$	effective thermal conductivity of the tissue phase ($W\,m^{-1}\,K^{-1}$)
Nu_s	Nusselt number at the organ's surface incorporating the local thermal non-equilibrium model
$Nu_{s,simp}$	Nusselt number at the organ's surface based on the local thermal equilibrium model
q	heat flux ($W\,m^{-2}$)
q_s	heat flux at the body organ surface ($W\,m^{-2}$)
$\dot{q}_{gen}$	heat generation within the biological tissue ($W\,m^{-3}$)
T	temperature (K)
T_a	arterial blood temperature entering the organ (K)
$T_{b,m}$	blood mean temperature (K)
T_c	body core temperature (K)
T_s	temperature of the body organ surface subject to an imposed heat flux (K)
u	blood velocity ($m\,s^{-1}$)
u_a	arterial blood velocity entering the organ ($m\,s^{-1}$)
x	longitudinal coordinate (m)
y	transverse coordinate (m)

Greek symbols

ε	porosity (volume fraction of the vascular space)
η	non-dimensional transverse coordinate, y/D
Φ	non-dimensional heat generation within the biological tissue, $(1-\varepsilon)D\dot{q}_{gen}/q_s$
κ	ratio of the effective blood thermal conductivity to that of the tissue, $k_{b,eff}/k_{t,eff}$
λ	parameter, $\sqrt{Bi(1+\kappa)/\kappa}$
ρ	blood density ($kg\,m^{-3}$)
θ	non-dimensional temperature, $k_{t,eff}(T-T_s)/q_sD$
$\theta_{b,m}$	non-dimensional blood mean temperature
θ_c	non-dimensional body core temperature, $k_{t,eff}\,(T_c - T_s)/q_sD$
$\Delta\theta$	non-dimensional temperature difference between tissue and blood phases
ω	blood perfusion rate (s^{-1})

Subscripts/superscripts

b	blood phase
b,m	blood mean
c	body core
eff	effective property
s	body organ surface subject to an imposed heat flux
t	tissue phase

Symbol

$\langle\ \rangle$	intrinsic volume average of a quantity

throughout the body, and for frequently recurring tumor types. Localized hyperthermia treatment can be managed so as to have a relatively limited effect on healthy cells while a higher temperature is achieved in the cancer cells. In fact, one of the important issues in hyperthermia is to apply the treatment mainly on the abnormal cells to prevent burning and destroying the healthy ones. Hyperthermia is performed utilizing various techniques such as warm water bath balloons and blankets, hot wax, inductive coils (similar to those in electric blankets), and thermal chambers. For deep localized treatments various modalities such as short waves, ultra-high frequency sound waves, microwave and laser can be utilized.

Heat transport through the biological tissues, represented by bioheat models, involves thermal conduction in tissue and vascular system, blood–tissue convection and perfusion (through capillary tubes within the tissues) and also metabolic heat generation. Assuming local thermal equilibrium between the blood and the tissue, Pennes [16] presented one of the early and more frequently used bioheat models. Due to simplifications and shortcomings of this model, other workers have established mathematical bioheat models by extending or modifying Pennes model [17,18]. Wulff [19] modified the bioheat model's perfusion term, utilizing local mean blood velocity and tissue temperature gradient rather than the blood perfusion volumetric rate and the blood temperature difference, respectively, as used in Pennes model. Klinger [20] considered the local blood mass flux to modify the Pennes model. Chen and Holmes [21] developed the previously stated models considering the thermal equilibrium effects and adding the dispersion and microcirculatory perfusion terms. Analytical and computational studies have been done utilizing stated bioheat transfer models and the local thermal equilibrium assumption between the blood and the tissue [22–26]. Some bioheat models are also established and examined for countercurrent heat transfer in arterial-venous vessels [27–36].

Advantages of utilizing porous media theory in modeling bioheat transfer, due to fewer assumptions as compared to different established bioheat transfer models, are stressed by Khaled and Vafai [37], Nakayama and Kuwahara [38], and Khanafer and Vafai [39,40]. The biological structure can be treated as a blood saturated porous matrix including cells and interstices, the so-called tissue. Utilizing the porous media theory, non-thermal equilibrium between the blood and the tissue is addressed and the blood–tissue convective heat exchange is taken into account. Volume averaging over each of the blood and tissue phases results in an energy equation for each individual phase [41–50], known as the local thermal non-equilibrium model. The volume averaging over a representative elementary volume containing both the blood and the tissue phases results in a local thermal equilibrium model referred to as the one equation model. Description of the established bioheat transport models can be found in the literature [17,37,38,51]. A comprehensive synthesis and analysis of mathematical models representing bioheat transport has been recently presented by Khanafer and Vafai [39]. Further, the analytical characterization and production of an isothermal surface for biological and electronics applications is given in Mahjoob and Vafai [52].

As mentioned earlier, the knowledge of the heat transfer process within the blood perfused tissues and the temperature distribution in tissues and organs are essential for an effective thermal therapy such as hyperthermia cancer treatment and also reducing any undesired effect on the healthy cells. In this work, the thermal therapy and heat flux intensity effects on the biological media are investigated and characterized analytically to establish a more accurate prediction of the blood and tissue temperature distributions within biological organs, applicable in bioheat applications such as hyperthermia. Utilizing the local thermal non-equilibrium model of porous media theory, exact solutions for the tissue and blood temperature distributions are established. These exact solutions can be utilized for different types of tissues and organs while determining the physical condition of the patient by considering effective parameters such as the vascular volume fraction, tissue matrix permeability and size, blood pressure and velocity, metabolic heat generation, imposed heat flux, and body core temperature. As such, the current models for temperature prediction during thermal therapies can be modified to present a more accurate temperature distribution within healthy and diseased cells.

2. Modeling and formulation

2.1. Problem description

Biological media usually consist of blood vessels, cells, and interstitial space, which can be, categorized as vascular and extra-vascular regions (Fig. 1a). As such, a biological structure can be modeled as a porous matrix, including cells and interstitial space, called tissue in which the blood infiltrates through. In this work, the blood and tissue local heat exchange, while the biological media is subjected to an imposed heat flux as in hyperthermia, is addressed and the blood and tissue temperature profiles are established analytically. The established analytical correlations incorporate the effects of the imposed heat flux, blood and tissue physical properties, arterial blood velocity, porosity and geometrical properties of the biological structure, internal heat generation within the tissue (e.g. metabolic heat generation), and the heat penetration depth. Two primary conditions are investigated in this work to simulate bioheat transport through a biological structure. In the first model, an isolated boundary condition exists at a depth (D) across which the heat can penetrate. This model is also applicable as a symmetry thermal boundary condition in which the heat flux is imposed from both sides of the organ (Fig. 1b). The second model is based on the physical representation of the core tissue/organ at a safe value at depth (D) through imposition of a uniform temperature at that depth. Flow is assumed to be hydraulically and thermally fully developed. Natural convection and radiation are assumed to be negligible and thermodynamic properties of the tissue and blood are considered to be temperature independent.

2.2. Governing equations

The anatomic structure is modeled as a porous medium consisting of the blood and the tissue (solid matrix) phases. The governing energy equations for the blood and tissue phases incorporating internal heat sources (e.g. metabolic reactions) and local thermal non-equilibrium conditions can be represented as [37–39,41–49].

Blood phase:

$$k_{\mathrm{b,eff}}\nabla_y^2\langle T_\mathrm{b}\rangle^\mathrm{b} + h_{\mathrm{tb}}a_{\mathrm{tb}}(\langle T_\mathrm{t}\rangle^\mathrm{t} - \langle T_\mathrm{b}\rangle^\mathrm{b}) = \varepsilon\rho c_\mathrm{p}\langle u\rangle^\mathrm{b}\frac{\partial\langle T_\mathrm{b}\rangle^\mathrm{b}}{\partial x} \quad (1)$$

Tissue phase:

$$k_{\mathrm{t,eff}}\nabla_y^2\langle T_\mathrm{t}\rangle^\mathrm{t} - h_{\mathrm{tb}}a_{\mathrm{tb}}(\langle T_\mathrm{t}\rangle^\mathrm{t} - \langle T_\mathrm{b}\rangle^\mathrm{b}) + (1-\varepsilon)\dot{q}_{\mathrm{gen}} = 0 \quad (2)$$

where,

$$k_{\mathrm{b,eff}} = \varepsilon k_\mathrm{b} + k_{\mathrm{b,dis}} \quad (3)$$
$$k_{\mathrm{t,eff}} = (1-\varepsilon)k_\mathrm{t} \quad (4)$$

where, parameters $\langle T_\mathrm{b}\rangle^\mathrm{b}$, $\langle T_\mathrm{t}\rangle^\mathrm{t}$, $\langle u\rangle^\mathrm{b}$, $k_{\mathrm{b,eff}}$, $k_{\mathrm{t,eff}}$, k_b, k_t, $k_{\mathrm{b,dis}}$, ε, ρ, and c_p are the intrinsic phase average blood and tissue temperatures, intrinsic blood phase average velocity, blood and tissue effective thermal conductivities, blood and tissue thermal conductivities, blood dispersion thermal conductivity, porosity (the volume fraction of the vascular space), blood density and specific heat, respectively. The blood–tissue interfacial heat transfer coefficient is represented by h_{tb} and the specific surface area by a_{tb}, and $\dot{q}_{\mathrm{gen}}$ is the heat generation within the biological tissue (e.g. metabolic heat generation). Nakayama and Kuwahara [38] state that replacing the perfusion term of the simpler bioheat models by the interfacial convective heat transfer term in the porous media model should be examined and they proposed replacing the term $h_{\mathrm{tb}}a_{\mathrm{tb}}$ by $h_{\mathrm{tb}}a_{\mathrm{tb}} + \rho c_\mathrm{p}\omega$ in both the blood and tissue energy Eqs. (1) and (2). Parameter ω represents the blood perfusion rate, which can be considered independent of location and temperature for simplicity. As such, the established exact solutions in this work are general solutions, which can satisfy both cases of utilizing the perfusion term as stated in Nakayama and Kuwahara model [38] or without that modification.

2.3. Boundary conditions

The imposed heat flux at the organ's surface can be represented under the local thermal non-equilibrium conditions, based on the work of Amiri et al. [48], Lee and Vafai [45] and Marafie and Vafai [49] as

$$q_\mathrm{s} = -k_{\mathrm{b,eff}}\left.\frac{\partial\langle T_\mathrm{b}\rangle^\mathrm{b}}{\partial y}\right|_{y=0} - k_{\mathrm{t,eff}}\left.\frac{\partial\langle T_\mathrm{t}\rangle^\mathrm{t}}{\partial y}\right|_{y=0} \quad (5)$$

The temperature at the interface of the body organ surface is likely to be uniform regardless of whether it contacts the tissue solid matrix or the blood. As such the temperature of the tissue and the blood at the organ surface will be the same [45,48,49]:

$$\left.\langle T_\mathrm{b}\rangle^\mathrm{b}\right|_{y=0} \approx \left.\langle T_\mathrm{t}\rangle^\mathrm{t}\right|_{y=0} \approx T_\mathrm{s} \quad (6)$$

The external heat flux influences the tissue within a depth of D. As discussed earlier, two models are investigated for the boundary condition at the depth of D from the surface subject to a given heat flux. These are (I) isolated core region and (II) uniform core temperature (T_c) at depth (D) as shown in Fig. 1. The value of the uniform temperature (T_c) can be assigned as the body core temperature or a safe temperature not to damage the healthy tissues. These models are represented as

Model I: isolated core region condition

$$\left.\frac{\partial\langle T_\mathrm{b}\rangle^\mathrm{b}}{\partial y}\right|_{y=D} = \left.\frac{\partial\langle T_\mathrm{t}\rangle^\mathrm{t}}{\partial y}\right|_{y=D} = 0 \quad (7)$$

Model II: uniform core temperature condition

$$\left.\langle T_\mathrm{b}\rangle^\mathrm{b}\right|_{y=D} \approx \left.\langle T_\mathrm{t}\rangle^\mathrm{t}\right|_{y=D} \approx T_\mathrm{c} \quad (8)$$

2.4. Normalization

The governing equations are normalized utilizing the following non-dimensional variables:

$$\eta = \frac{y}{D},\quad \kappa = \frac{k_{\mathrm{b,eff}}}{k_{\mathrm{t,eff}}},\quad Bi = \frac{h_{\mathrm{tb}}a_{\mathrm{tb}}D^2}{k_{\mathrm{t,eff}}},\quad \theta = \frac{k_{\mathrm{t,eff}}(\langle T\rangle - T_\mathrm{s})}{q_\mathrm{s}D},$$
$$\Phi = \frac{(1-\varepsilon)D\dot{q}_{\mathrm{gen}}}{q_\mathrm{s}} \quad (9)$$

Utilizing Eqs. (5) and (7)–(9), the governing Eqs. (1) and (2) can be casted as

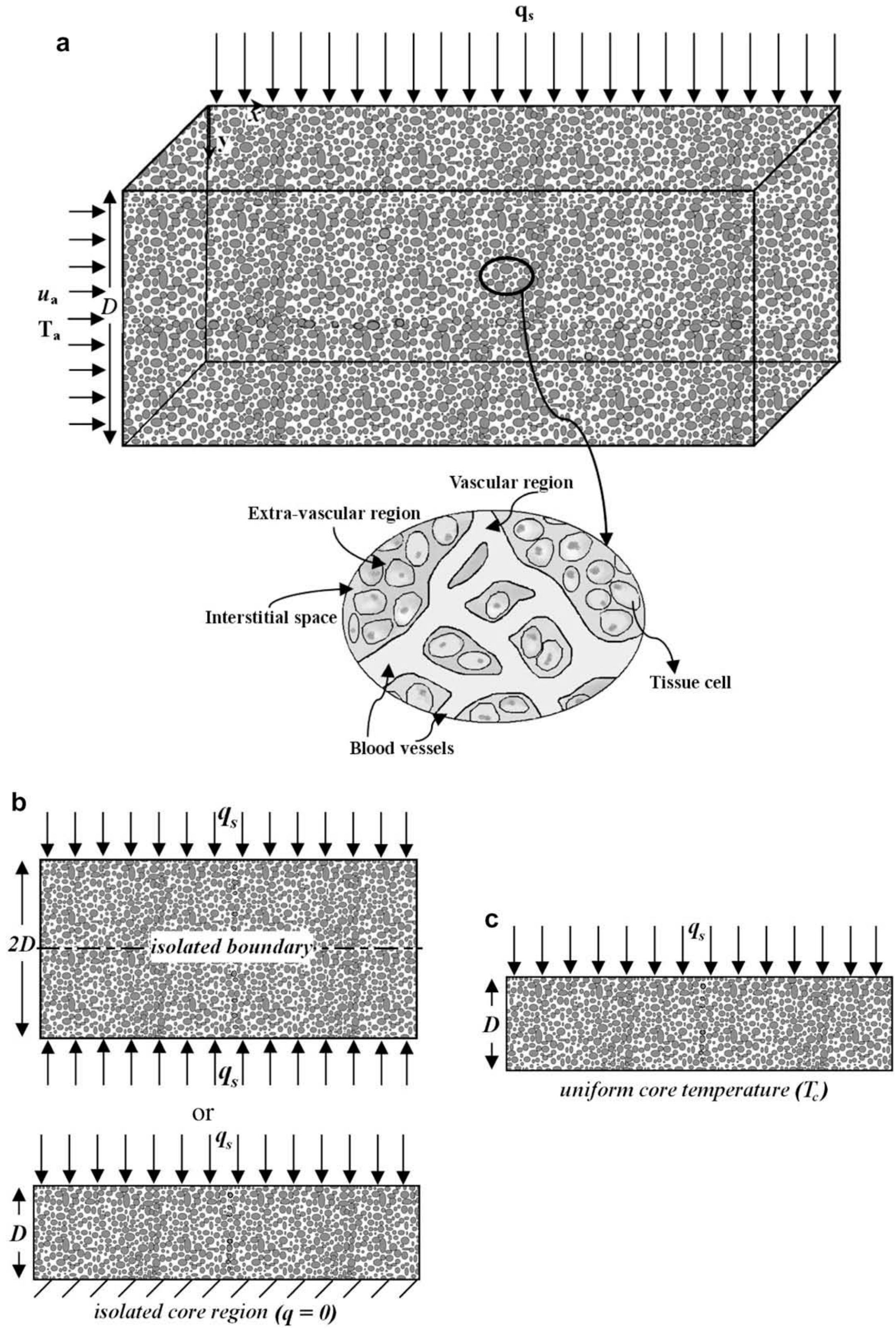

Fig. 1. Schematic diagram of (a) the tissue-vascular system, (b) Model I: peripheral heat flux or isolated core region condition, and (c) Model II: uniform core temperature condition.

$$\kappa\frac{\partial^4\theta_b}{\partial\eta^4}-(1+k)Bi\left(\frac{\partial^2\theta_b}{\partial\eta^2}\right)=\Lambda \tag{10}$$

$$\kappa\frac{\partial^4\theta_t}{\partial\eta^4}-(1+k)Bi\left(\frac{\partial^2\theta_t}{\partial\eta^2}\right)=\Lambda \tag{11}$$

in which,

$$\Lambda=-Bi \qquad \text{for model I : isolated core region condition} \tag{12}$$

$$\Lambda=-Bi(1+(1+\kappa)\theta_c) \qquad \text{for model II : uniform core temperature condition} \tag{13}$$

where,

$$\theta_c = \frac{k_{t,eff}(T_c - T_s)}{q_s D} \tag{14}$$

Furthermore, utilizing equation (9), the boundary conditions (6)–(8) can be normalized for each model. Additional boundary conditions to solve the obtained 4th order blood/tissue energy Eqs. (10) and (11) can be obtained by evaluating the second or third order derivatives of θ_b and θ_t at the boundaries. This results in the following set of boundary conditions for each model:

Model I: isolated core region condition

$$\theta_b|_{\eta=0} = \theta_t|_{\eta=0} = 0 \tag{15}$$

$$\left.\frac{\partial\theta_b}{\partial\eta}\right|_{\eta=1} = \left.\frac{\partial\theta_t}{\partial\eta}\right|_{\eta=1} = 0 \tag{16}$$

$$\left.\frac{\partial^2\theta_b}{\partial\eta^2}\right|_{\eta=0} = \frac{1+\Phi}{\kappa} \tag{17}$$

$$\left.\frac{\partial^2\theta_t}{\partial\eta^2}\right|_{\eta=0} = -\Phi \tag{18}$$

$$\left.\frac{\partial^3\theta_b}{\partial\eta^3}\right|_{\eta=1} = \left.\frac{\partial^3\theta_t}{\partial\eta^3}\right|_{\eta=1} = 0 \tag{19}$$

Model II: uniform core temperature condition

$$\theta_b|_{\eta=0} = \theta_t|_{\eta=0} = 0 \tag{20}$$

$$\theta_b|_{\eta=1} = \theta_t|_{\eta=1} = \theta_c \tag{21}$$

$$\left.\frac{\partial^2\theta_b}{\partial\eta^2}\right|_{\eta=0} = \left.\frac{\partial^2\theta_b}{\partial\eta^2}\right|_{\eta=1} = \frac{1+(1+\kappa)\theta_c+\Phi}{\kappa} \tag{22}$$

$$\left.\frac{\partial^2\theta_t}{\partial\eta^2}\right|_{\eta=0} = \left.\frac{\partial^2\theta_t}{\partial\eta^2}\right|_{\eta=1} = -\Phi \tag{23}$$

2.5. Blood, tissue, and surface temperature fields

Blood and tissue phase temperature distributions, can be obtained by solving the governing equations and utilizing the Neumann and Dirichlet boundary conditions given by Eqs. (10)–(23). After considerable analysis, it results in the blood and tissue temperature profiles (for the sake of simplicity, the volume averaging sign ($\langle\ \rangle$) is dropped):

Model I: isolated core region condition

$$\theta_b = \frac{1}{1+\kappa}\left(\eta\left(\frac{\eta}{2}-1\right) - \frac{1+(1+\kappa)\Phi}{(1+\kappa)Bi}\left\{1-\frac{e^{\lambda\eta}+e^{\lambda(2-\eta)}}{1+e^{2\lambda}}\right\}\right) \tag{24}$$

$$\theta_t = \frac{1}{1+\kappa}\left(\eta\left(\frac{\eta}{2}-1\right) + \frac{\kappa(1+(1+\kappa)\Phi)}{(1+\kappa)Bi}\left\{1-\frac{e^{\lambda\eta}+e^{\lambda(2-\eta)}}{1+e^{2\lambda}}\right\}\right) \tag{25}$$

where,

$$\lambda = \sqrt{Bi(1+\kappa)/\kappa} \tag{26}$$

As such, the temperature difference between the tissue and the blood phases and the blood mean temperature can be written as

$$\Delta\theta = \theta_t - \theta_b = \frac{1+(1+\kappa)\Phi}{(1+\kappa)Bi}\left(1-\frac{e^{\lambda\eta}+e^{\lambda(2-\eta)}}{1+e^{2\lambda}}\right) \tag{27}$$

$$\theta_{b,m} = \frac{-1}{1+\kappa}\left(\frac{1}{3} + \frac{1+(1+\kappa)\Phi}{(1+\kappa)Bi}\left\{1-\frac{1}{\lambda}\frac{e^{2\lambda}-1}{e^{2\lambda}+1}\right\}\right) \tag{28}$$

The dimensional blood mean temperature and the body organ surface temperature which is subjected to an imposed heat flux, are derived to be

$$T_{b,m} = \frac{q_s + (1-\varepsilon)D\dot{q}_{gen}}{\rho c_p u_a D}x + T_a \tag{29}$$

$$T_s = \frac{q_s + (1-\varepsilon)D\dot{q}_{gen}}{\rho c_p u_a D}x + \frac{q_s D}{k_{t,eff}(1+\kappa)} \times\left(\frac{1}{3} + \frac{q_s + (1-\varepsilon)(1+\kappa)D\dot{q}_{gen}}{(1+\kappa)Biq_s}\left\{1-\frac{1}{\lambda}\frac{e^{2\lambda}-1}{e^{2\lambda}+1}\right\}\right) + T_a \tag{30}$$

Finally, using Eqs. (9), (24), (25) and (30), the blood and tissue temperature profiles can be casted as

$$T_b = \frac{q_s y}{k_{t,eff}(1+\kappa)}\left(\frac{y}{2D}-1\right) + \frac{q_s D + (1-\varepsilon)(1+\kappa)D^2\dot{q}_{gen}}{k_{t,eff}(1+\kappa)^2 Bi}\left\{\frac{e^{2\lambda}(\lambda e^{-\lambda y/D}-1)+\lambda e^{\lambda y/D}+1}{\lambda(e^{2\lambda}+1)}\right\} + \frac{q_s + (1-\varepsilon)D\dot{q}_{gen}}{\rho c_p u_a D}x + \frac{q_s D}{3k_{t,eff}(1+\kappa)} + T_a \tag{31}$$

$$T_t = \frac{q_s y}{k_{t,eff}(1+\kappa)}\left(\frac{y}{2D}-1\right) + \frac{q_s D + (1-\varepsilon)(1+\kappa)D^2\dot{q}_{gen}}{k_{t,eff}(1+\kappa)^2 Bi} \times\left\{(1+\kappa) - \frac{e^{2\lambda}(\kappa\lambda e^{-\lambda y/D}+1)+\kappa\lambda e^{\lambda y/D}-1}{\lambda(e^{2\lambda}+1)}\right\} + \frac{q_s + (1-\varepsilon)D\dot{q}_{gen}}{\rho c_p u_a D}x + \frac{q_s D}{3k_{t,eff}(1+\kappa)} + T_a \tag{32}$$

Model II: uniform core temperature condition

$$\theta_b = \frac{1}{1+\kappa}\left(\frac{\eta}{2}[(1+(1+\kappa)\theta_c)\eta + (1+\kappa)\theta_c - 1] - \frac{(1+\kappa)(\theta_c+\Phi)+1}{(1+\kappa)Bi}\left\{1-\frac{e^{\lambda\eta}+e^{\lambda(1-\eta)}}{1+e^{\lambda}}\right\}\right) \tag{33}$$

$$\theta_t = \frac{1}{1+\kappa}\left(\frac{\eta}{2}[(1+(1+\kappa)\theta_c)\eta + (1+\kappa)\theta_c - 1] + \frac{\kappa[(1+\kappa)(\theta_c+\Phi)+1]}{(1+\kappa)Bi}\left\{1-\frac{e^{\lambda\eta}+e^{\lambda(1-\eta)}}{1+e^{\lambda}}\right\}\right) \tag{34}$$

where,

$$\lambda = \sqrt{Bi(1+\kappa)/\kappa}$$

and

$$\Delta\theta = \theta_t - \theta_b = \frac{(1+\kappa)(\theta_c+\Phi)+1}{(1+\kappa)Bi}\left\{1-\frac{e^{\lambda\eta}+e^{\lambda(1-\eta)}}{1+e^{\lambda}}\right\} \tag{35}$$

$$\theta_{b,m} = \frac{-1}{1+\kappa}\left(\frac{1-5(1+\kappa)\theta_c}{12} + \frac{1+(1+\kappa)(\theta_c+\Phi)}{(1+\kappa)Bi}\left\{1-\frac{2}{\lambda}\frac{e^{\lambda}-1}{e^{\lambda}+1}\right\}\right) \tag{36}$$

The blood mean temperature and the organ surface temperature, which is subjected to an imposed heat flux, are derived to be

$$T_{b,m} = \left(T_a - T_c - \frac{q_s D}{k_{t,eff}(1+\kappa)}\left(\frac{1}{2} + \frac{(1-\varepsilon)D\dot{q}_{gen}}{q_s} \times\left\{\frac{7}{12} - \frac{\kappa}{Bi(1+\kappa)}\left(1-\frac{2(e^{\lambda}-1)}{\lambda(e^{\lambda}+1)}\right)\right\}\right)\right) \times \exp\left[\frac{-12Bik_{t,eff}(1+\kappa)^2 x}{\rho c_p u_a D^2\left(7Bi(1+\kappa)+12\left(1-\frac{2(e^{\lambda}-1)}{\lambda(e^{\lambda}+1)}\right)\right)}\right] + \frac{q_s D}{k_{t,eff}(1+\kappa)}\left(\frac{1}{2} + \frac{(1-\varepsilon)D\dot{q}_{gen}}{q_s}\left[\frac{7}{12} - \frac{\kappa\left(1-\frac{2(e^{\lambda}-1)}{\lambda(e^{\lambda}+1)}\right)}{Bi(1+\kappa)}\right]\right) + T_c \tag{37}$$

$$T_s = \left(\frac{T_a - T_c - \frac{q_s D}{k_{t,eff}(1+\kappa)} \left(\frac{1}{2} + \frac{(1-\varepsilon)D\dot{q}_{gen}}{q_s} \left\{ \frac{7}{12} - \frac{\kappa}{Bi(1+\kappa)} \left(1 - \frac{2(e^{\lambda}-1)}{\lambda(e^{\lambda}+1)} \right) \right\} \right)}{\frac{7}{12} + \frac{1}{Bi(1+\kappa)} \left(1 - \frac{2(e^{\lambda}-1)}{\lambda(e^{\lambda}+1)} \right)} \right) \times \exp\left[\frac{-12Bik_{t,eff}(1+\kappa)^2 x}{\rho c_p u_a D^2 \left(7Bi(1+\kappa) + 12\left(1 - \frac{2(e^{\lambda}-1)}{\lambda(e^{\lambda}+1)} \right) \right)} \right] + \frac{q_s D + (1-\varepsilon)D^2\dot{q}_{gen}}{k_{t,eff}(1+\kappa)} + T_c \tag{38}$$

Using Eqs. (9), (33), (34) and (38), the blood and tissue temperature profiles can be casted as

$$T_b = \frac{q_s}{k_{t,eff}(1+\kappa)}(D-y) + \frac{(1-\varepsilon)D^2\dot{q}_{gen}}{k_{t,eff}(1+\kappa)} \left(1 - \frac{y}{2D}\left(\frac{y}{D}+1\right) - \frac{\kappa}{Bi(1+\kappa)} \left\{ 1 - \frac{e^{\lambda y/D} + e^{\lambda(1-\frac{y}{D})}}{1+e^{\lambda}} \right\} \right) + \left(1 - \frac{y}{2D}\left(\frac{y}{D}+1\right) + \frac{1}{Bi(1+\kappa)} \left\{ 1 - \frac{e^{\lambda y/D} + e^{\lambda(1-\frac{y}{D})}}{1+e^{\lambda}} \right\} \right) \times \left(\frac{T_a - T_c - \frac{q_s D}{k_{t,eff}(1+\kappa)} \left(\frac{1}{2} + \frac{(1-\varepsilon)D\dot{q}_{gen}}{q_s} \left\{ \frac{7}{12} - \frac{\kappa}{Bi(1+\kappa)} \times \left(1 - \frac{2(e^{\lambda}-1)}{\lambda(e^{\lambda}+1)} \right) \right\} \right)}{\frac{7}{12} + \frac{1}{Bi(1+\kappa)} \left(1 - \frac{2(e^{\lambda}-1)}{\lambda(e^{\lambda}+1)} \right)} \right) \times \exp\left[\frac{-12Bik_{t,eff}(1+\kappa)^2 x}{\rho c_p u_a D^2 \left(7Bi(1+\kappa) + 12\left(1 - \frac{2(e^{\lambda}-1)}{\lambda(e^{\lambda}+1)} \right) \right)} \right] + T_c \tag{39}$$

$$T_t = \frac{q_s}{k_{t,eff}(1+\kappa)}(D-y) + \frac{(1-\varepsilon)D^2\dot{q}_{gen}}{k_{t,eff}(1+\kappa)} \left(1 - \frac{y}{2D}\left(\frac{y}{D}+1\right) + \frac{\kappa^2}{Bi(1+\kappa)} \left\{ 1 - \frac{e^{\lambda y/D} + e^{\lambda(1-\frac{y}{D})}}{1+e^{\lambda}} \right\} \right) + \left(1 - \frac{y}{2D}\left(\frac{y}{D}+1\right) - \frac{k}{Bi(1+\kappa)} \left\{ 1 - \frac{e^{\lambda y/D} + e^{\lambda(1-\frac{y}{D})}}{1+e^{\lambda}} \right\} \right) \times \left(\frac{T_a - T_c - \frac{q_s D}{k_{t,eff}(1+\kappa)} \left(\frac{1}{2} + \frac{(1-\varepsilon)D\dot{q}_{gen}}{q_s} \left\{ \frac{7}{12} - \frac{\kappa}{Bi(1+\kappa)} \times \left(1 - \frac{2(e^{\lambda}-1)}{\lambda(e^{\lambda}+1)} \right) \right\} \right)}{\frac{7}{12} + \frac{1}{Bi(1+\kappa)} \left(1 - \frac{2(e^{\lambda}-1)}{\lambda(e^{\lambda}+1)} \right)} \right) \times \exp\left[\frac{-12Bik_{t,eff}(1+\kappa)^2 x}{\rho c_p u_a D^2 \left(7Bi(1+\kappa) + 12\left(1 - \frac{2(e^{\lambda}-1)}{\lambda(e^{\lambda}+1)} \right) \right)} \right] + T_c \tag{40}$$

It should be noted that utilizing the established organ surface temperature correlation (Eqs. (30) and (38)), a relationship between the heat flux value, depth of heat penetration and surface temperature are established in which having two of these quantities, the third one can be evaluated.

2.6. Heat transfer correlations

The body organ surface heat transfer coefficient for the local thermal non-equilibrium model is obtained from

$$h_s = \frac{q_s}{T_s - T_{b,m}} \tag{41}$$

As such, the heat exchange rate represented by a Nusselt number at the body organ surface subject to an imposed heat flux (q_s) can be displayed as

$$Nu_s = \frac{h_s D_h}{k_{b,eff}} = \frac{-2}{\kappa\theta_{b,m}} \tag{42}$$

Utilizing Eqs. (28) and (36), the Nusselt number can be represented as

Model I: isolated core region condition

$$Nu_s = \frac{6(1+\kappa)/\kappa}{1 + \frac{3q_s + 3(1+\kappa)(1-\varepsilon)D\dot{q}_{gen}}{(1+\kappa)Biq_s} \left(1 - \frac{1}{\lambda} \frac{e^{2\lambda}-1}{e^{2\lambda}+1} \right)} \tag{43}$$

Model II: uniform core temperature condition

$$Nu_s = \frac{24(1+\kappa)/\kappa}{\left\{ \begin{array}{l} \left(\frac{12k_{t,eff}(1+\kappa)(T_a - T_c)}{q_s D} - \left(6 + \frac{(1-\varepsilon)D\dot{q}_{gen}}{q_s} \left\{ 7 - \frac{12\kappa}{Bi(1+\kappa)} \left(1 - \frac{2(e^{\lambda}-1)}{\lambda(e^{\lambda}+1)} \right) \right\} \right) \right) \\ \times \left(\frac{12Bi(1+\kappa)}{7Bi(1+\kappa) + 12\left(1 - \frac{2(e^{\lambda}-1)}{\lambda(e^{\lambda}+1)} \right)} - 1 \right) \exp\left[\frac{-12Bik_{t,eff}(1+\kappa)^2 x}{\rho c_p u_a D^2 \left(7Bi(1+\kappa) + 12\left(1 - \frac{2(e^{\lambda}-1)}{\lambda(e^{\lambda}+1)} \right) \right)} \right] \\ +6 + \frac{(1-\varepsilon)D\dot{q}_{gen}}{q_s} \left[5 + \frac{12\kappa}{(1+\kappa)Bi} \left(1 - \frac{2(e^{\lambda}-1)}{\lambda(e^{\lambda}+1)} \right) \right] \end{array} \right\}} \tag{44}$$

2.7. Simplified solution

A simplified solution can be obtained assuming thermal equilibrium between the blood and tissue phases, i.e., $\theta = \theta_b = \theta_t$. Adding the energy equations and utilizing boundary conditions (5)–(8), the blood and tissue temperature distributions and the Nusselt number are obtained as

Model I: isolated core region condition

$$\theta = \frac{\eta}{1+\kappa}\left(\frac{\eta}{2} - 1 \right) \tag{45}$$

$$T_{b,m} = \frac{q_s + (1-\varepsilon)D\dot{q}_{gen}}{\rho c_p u_a D} x + T_a$$

$$T_s = \frac{q_s + (1-\varepsilon)D\dot{q}_{gen}}{\rho c_p u_a D} x + \frac{q_s D}{3k_{t,eff}(1+\kappa)} + T_a \tag{46}$$

$$T_b = T_t = \frac{q_s y}{k_{t,eff}(1+\kappa)}\left(\frac{y}{2D} - 1 \right) + \frac{q_s + (1-\varepsilon)D\dot{q}_{gen}}{\rho c_p u_a D} x + \frac{q_s D}{3k_{t,eff}(1+\kappa)} + T_a \tag{47}$$

$$Nu_{s,simp} = 6\frac{1+\kappa}{\kappa} \tag{48}$$

Model II: uniform core temperature condition

$$\theta = \frac{\eta}{2(1+\kappa)}[(1 + (1+\kappa)\theta_c)\eta + (1+\kappa)\theta_c - 1] \tag{49}$$

$$T_{b,m} = \left(T_a - T_c - \frac{q_s D}{k_{t,eff}(1+\kappa)}\left(\frac{1}{2} + \frac{7(1-\varepsilon)D\dot{q}_{gen}}{12q_s} \right) \right) \times \exp\left(\frac{-12k_{t,eff}(1+\kappa)x}{7\rho c_p u_a D^2} \right) + \frac{q_s D}{2k_{t,eff}(1+\kappa)} \times \left(1 + \frac{7(1-\varepsilon)D\dot{q}_{gen}}{6q_s} \right) + T_c \tag{50}$$

$$T_s = \left(\frac{12}{7}(T_a - T_c) - \frac{q_s D}{k_{t,eff}(1+\kappa)}\left(\frac{6}{7} + \frac{(1-\varepsilon)D\dot{q}_{gen}}{q_s} \right) \right) \times \exp\left(\frac{-12k_{t,eff}(1+\kappa)x}{7\rho c_p u_a D^2} \right) + \frac{q_s D + (1-\varepsilon)D^2\dot{q}_{gen}}{k_{t,eff}(1+\kappa)} + T_c \tag{51}$$

$$T_b = T_t = \left\{ \frac{12}{7}(T_a - T_c) - \frac{q_s D}{k_{t,eff}(1+\kappa)}\left(\frac{6}{7} + \frac{(1-\varepsilon)D\dot{q}_{gen}}{q_s} \right) \right\} \times \left(1 - \frac{y}{2D}\left(\frac{y}{D} + 1 \right) \right) \exp\left(\frac{-12k_{t,eff}(1+\kappa)x}{7\rho c_p u_a D^2} \right) + \frac{q_s}{k_{t,eff}(1+\kappa)}(D-y) + \frac{(1-\varepsilon)D^2\dot{q}_{gen}}{k_{t,eff}(1+\kappa)}\left(1 - \frac{y}{2D}\left(\frac{y}{D} + 1 \right) \right) + T_c \tag{52}$$

$$Nu_{s,simp} = \frac{24(1+\kappa)/\kappa}{\left(\frac{60k_{t,eff}(1+\kappa)}{7q_s D}(T_a - T_c) - \frac{5(1-\varepsilon)D\dot{q}_{gen}}{q_s} - \frac{30}{7} \right) \exp\left(\frac{-12k_{t,eff}(1+\kappa)x}{7\rho c_p u_a D^2} \right) + \frac{5(1-\varepsilon)D\dot{q}_{gen}}{q_s} + 6} \tag{53}$$

3. Results and discussions

The ability to readily and interactively predict tissue and blood temperature distributions within a body organ is crucial for an effective thermal therapy such as hyperthermia cancer treatment. The tissue and blood temperature profiles obtained from the present analytical correlations effectively address this need. The tissue and blood properties are utilized to assess the blood and tissue temperature distributions obtained from the present analytical results. Based on the cited values in the literature [39], a representative volume fraction (0.1 or less) of the vascular system is utilized for some of the comparisons. However, the established analytical expressions allow for incorporating variations in representative volume fraction as well as various physical attributes. In Figs. 2 and 3, the temperature profiles are compared with the available data in the literature. In the works of Lee and Vafai [45] and Marafie and Vafai [49], exact solutions for forced convective flow through a channel filled with a porous medium and subject to an imposed heat flux are established which is equivalent to model I of the present study (isolated core region condition) when the metabolic heat generation is zero.

In Fig. 2, the solid and liquid temperature profiles are compared with the results obtained from the analytical correlations established by Lee and Vafai [45] for the porosity of 0.1. The solid and liquid phase temperature distributions are in excellent agreement with the ones by Lee and Vafai [45] for a wide range of liquid–solid interstitial heat exchange parameters. Fig. 2 also indicates that a decrease in the internal heat exchange results in a larger blood and tissue temperature difference while displaying the importance of utilizing the local thermal non-equilibrium model. In Fig. 3, the solid and liquid temperature profiles obtained from the present analytical study are compared with the analytical results of Lee and Vafai [45] and analytical and numerical results of Marafie and Vafai [49] for the porosity of 0.01. A very good agreement is observed for all of the cited comparisons. The very small deviation between the numerical and analytical results is due to utilization of a smaller Darcy number in the numerical simulations [49].

In Fig. 4, the analytical temperature distribution is compared with the numerical results for both isolated and uniform core temperature condition models. For the numerical simulations, an implicit, pressure-based, cell-centered finite volume method is utilized to solve the coupled governing equations. The governing equations, including Darcy–Brinkman momentum equation and the energy equation with local thermal equilibrium assumption, are discretized and linearized utilizing second order upwind method for the convection term and central differencing for the diffusion terms. Resulting algebraic equations are solved sequentially using Gauss–Seidel point implicit linear equation solver in conjunction with an algebraic multi-grid (AMG) method in order to reduce the dispersion errors while increasing the computational speed. SIMPLE algorithm is utilized for the pressure–velocity coupling [53,54]. An iterative procedure utilizing under-relaxation is used and convergence is assumed when residuals become less than 10^{-6}. Comparing analytical and numerical results for both models indicates a very good qualitative and quantitative agreement as seen in Fig. 4.

Fig. 5 displays the effect of vascular volume fraction on the blood and tissue temperature profiles. As can be seen, in both isolated and uniform surface temperature models, a decrease in the vascular volume fraction increases the difference between the blood/tissue temperature and that of the body organ surface. As such, more temperature uniformity can be achieved within a biological structure with a larger vascular volume fraction resulting in a more effective hyperthermia treatment. A change in the vascular volume fraction also translates in a change in the blood and tissue effective thermal conductivities. The results in Fig. 5 display the cooling effect of the blood on the tissue–vascular system. As a natural cooling system in the body, the blood regulates the body temperature during hyperthermia treatment by arterial blood with the cold body core temperature, while modifying the vascular volume fraction of the biological structure. The natural body thermal regulation system increases or decreases the vascular volume fraction of the biological structure when exposed to a higher or lower temperature, respectively.

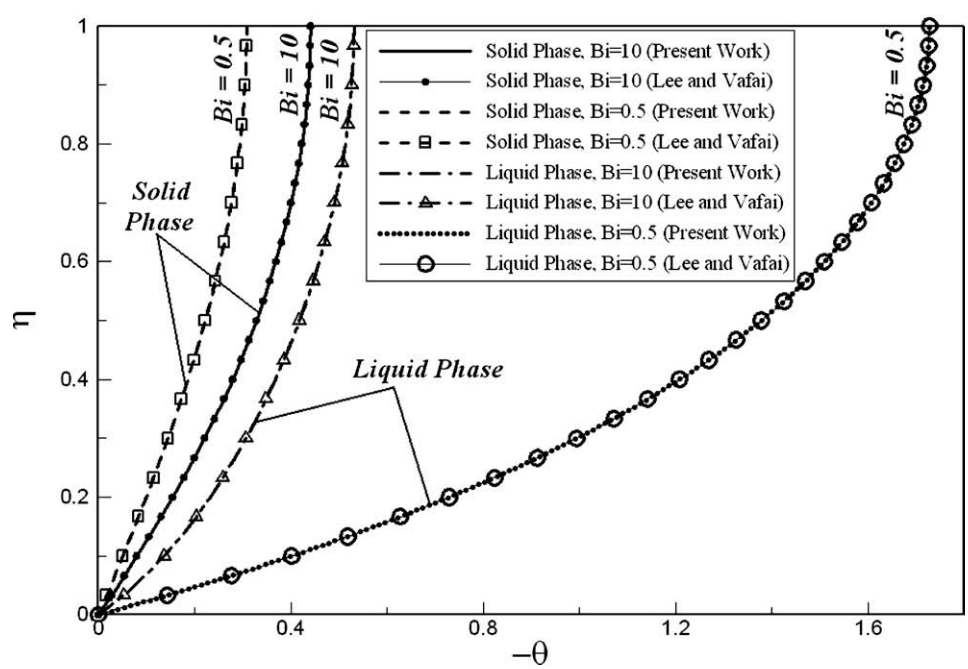

Fig. 2. Liquid and solid temperature profiles obtained from the present analytical solution and the analytical solution by Lee and Vafai [45] for Model I (isolated core region condition) for different interstitial heat exchange values and $\varepsilon = 0.1$, $\Phi = 0$, and $\kappa = 0.111$.

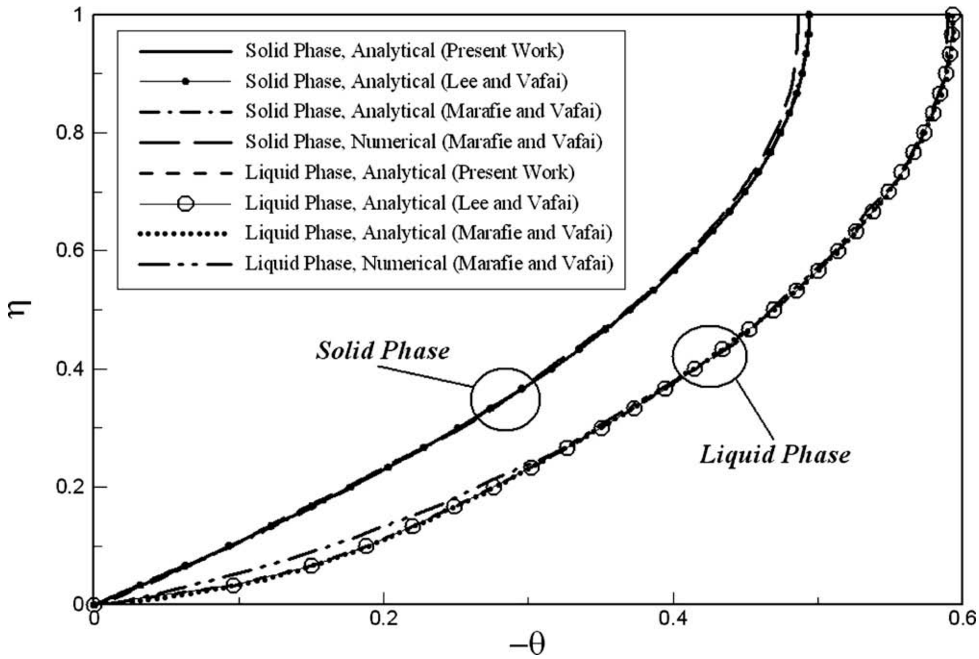

Fig. 3. Comparison of the liquid and solid temperature profiles obtained from the present analytical solution, the analytical solution by Lee and Vafai [45], and the analytical and numerical solutions by Marafie and Vafai [49] for Model I (isolated core region condition) at $Bi = 10$, $\varepsilon = 0.01$, $\Phi = 0$, and $\kappa = 0.01$.

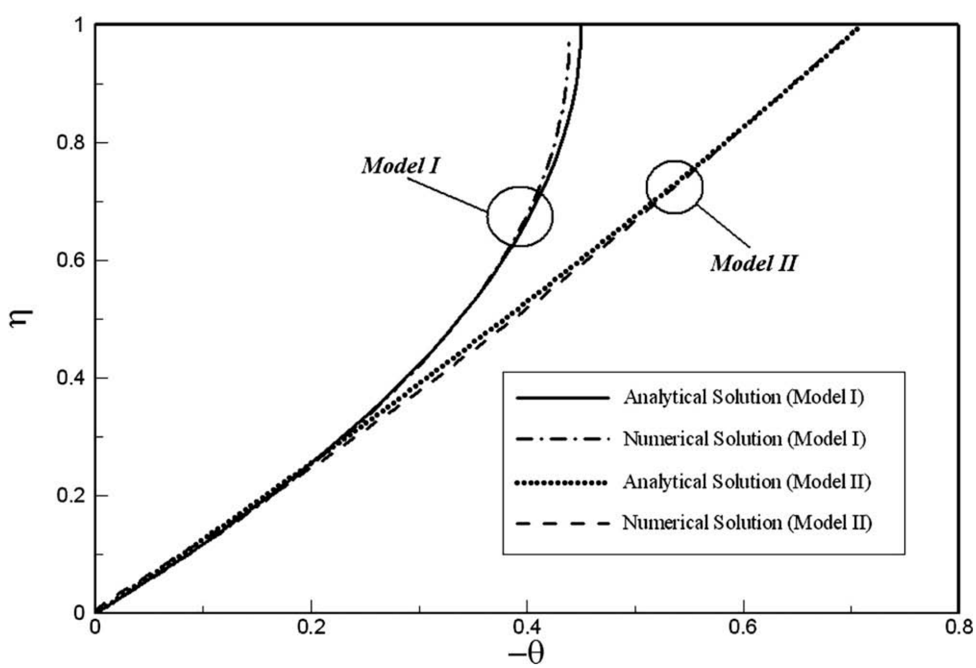

Fig. 4. Comparison of the temperature profile obtained from the present analytical and numerical solutions utilizing blood–tissue local thermal equilibrium assumption at $\varepsilon = 0.1$, $\Phi = 0.018$, and $\kappa = 0.111$.

Fig. 6 displays the effect of metabolic heat generation on the blood and tissue temperature profiles. As expected, larger heat generation ratio also results in higher temperatures in the organ as well as the blood within it. Fig. 6 confirms that, in both isolated and uniform core temperature models, an increase in the metabolic heat generation results in a larger deviation between the tissue temperature and that of the blood. This shows that then error in utilizing a local thermal equilibrium model for bioheat transfer investigations increases as the metabolic heat generation (Φ) increases.

4. Conclusions

Understanding heat transfer processes and temperature distributions within biological media are key issues in thermal therapy techniques such as hyperthermia cancer treatment. The biological media can be treated as a blood saturated tissue represented by a porous matrix. In this work, utilizing local thermal non-equilibrium model in porous media theory, exact solutions are established, for the first time, for the tissue and blood temperature

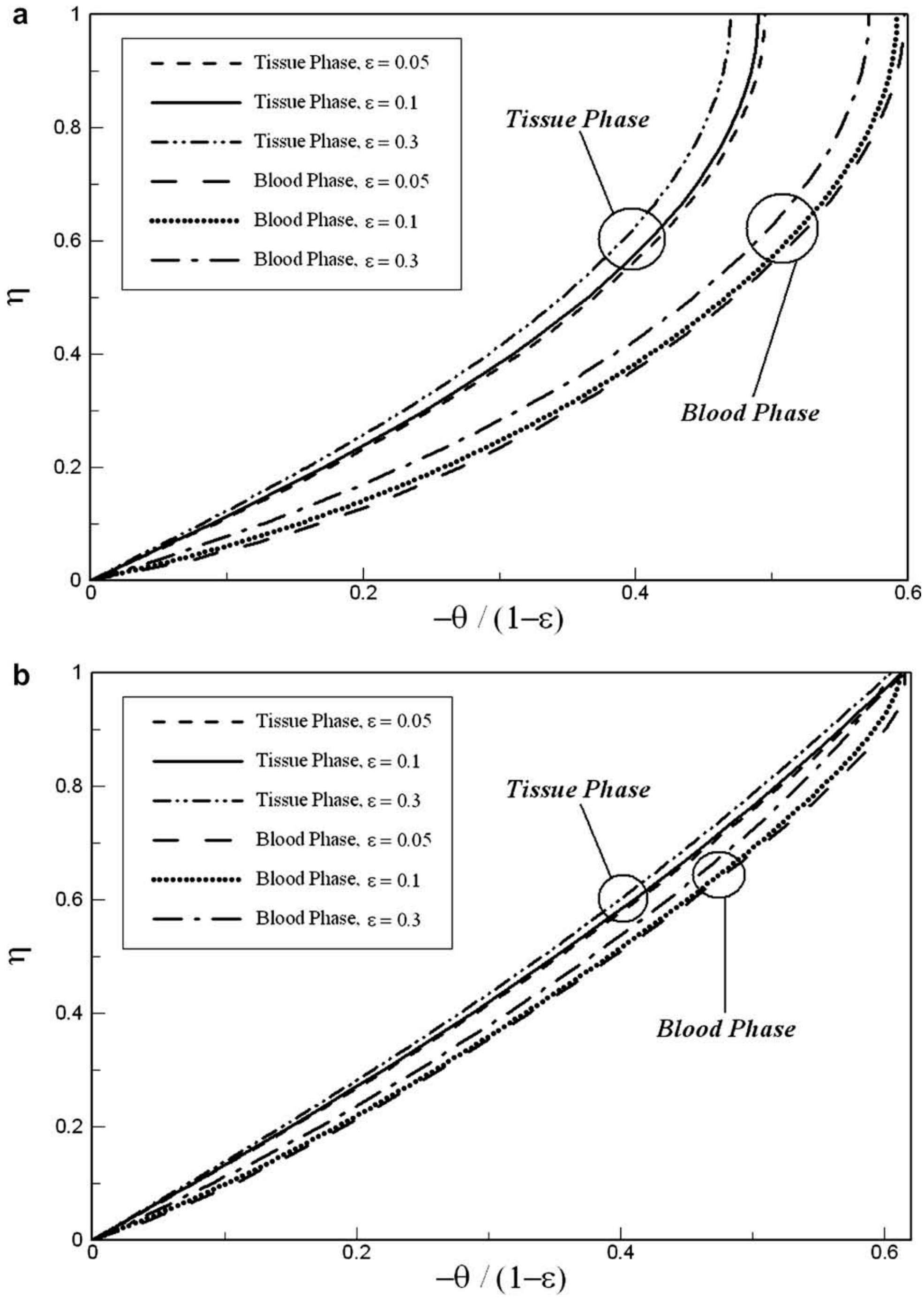

Fig. 5. The effect of vascular volume fraction on the blood and tissue temperature profiles at $Bi = 10$ and $\Phi/(1-\varepsilon) = 0.022$. (a) Model I: isolated core region condition and (b) Model II: uniform core temperature condition.

distributions for two tissue/organ models representing isolated and uniform core conditions. Analytical temperature distributions for the organ surface, subject to an imposed heat flux, and the blood mean temperature as well as overall heat exchange correlations are also presented incorporating the effective parameters such as the volume fraction of the vascular system, the blood and tissue thermal conductivities, interfacial blood–tissue heat exchange, tissue/organ depth, arterial velocity and temperature, body core temperature, imposed hyperthermia heat flux, metabolic heat generation, and the blood's physical properties. The exact solutions established in this work allow for a readily accessible and interactive prediction of tissue and blood temperature distribution within a body organ. This addresses a crucial need in hyperthermia treatment. A very good agreement exists between the results, obtained from the present analytical study, and the available data in the literature and our numerical simulations. The results indicate the importance of utilizing the local thermal non-equilibrium model especially at higher metabolic heat generation ratios (Φ) and within biological media with lower vascular volume fraction. A decrease in the metabolic heat generation or an increase in the organ/tissue's vascular volume fraction enhances temperature uniformity within the media resulting in a more effective hyperthermia treatment. Simplified solutions were also established based on the local thermal equilibrium between the tissue

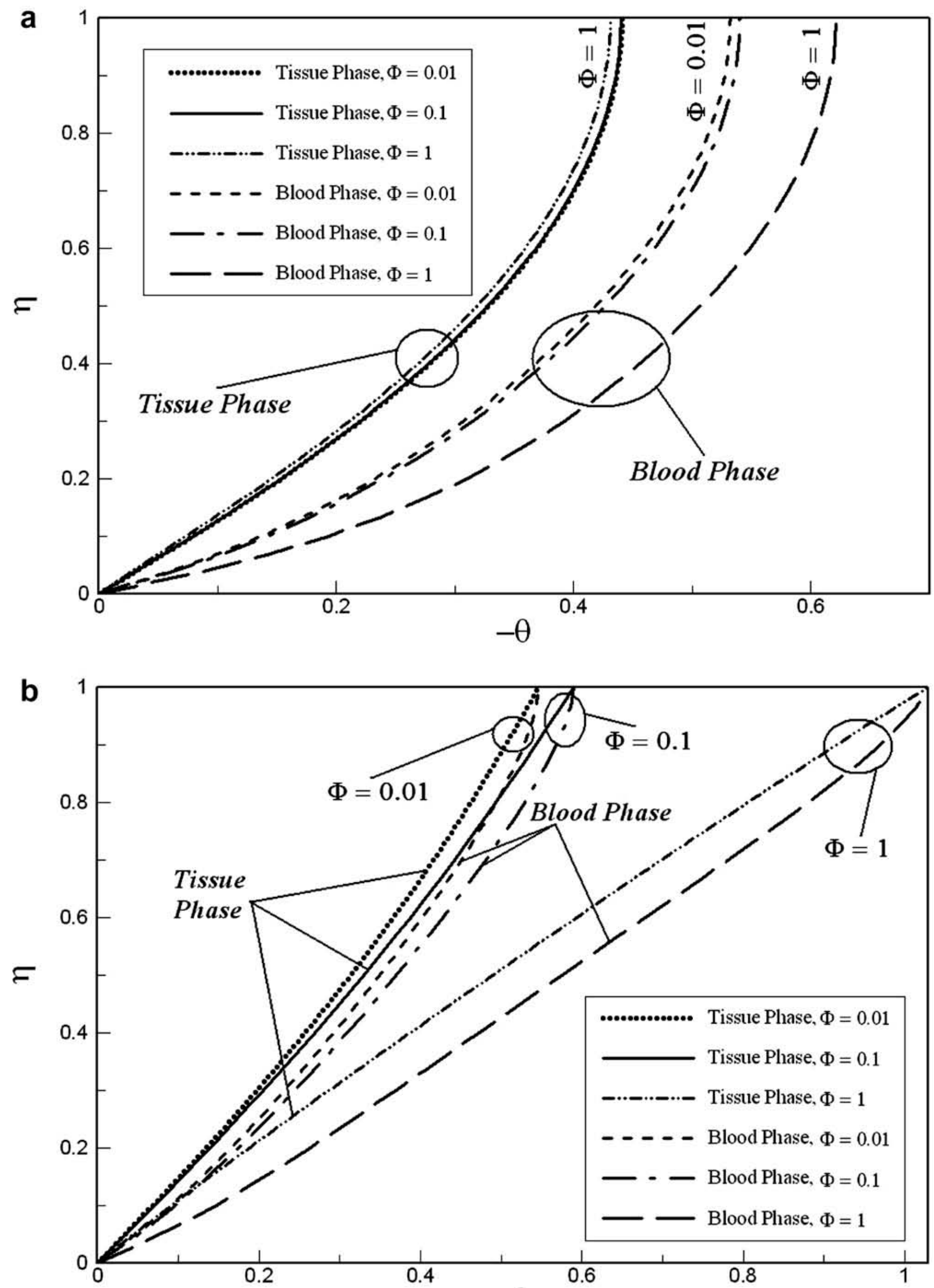

Fig. 6. The effect of metabolic heat generation on the blood and tissue temperature profiles at $Bi = 10$, $\varepsilon = 0.1$, and $\kappa = 0.111$. (a) Model I: isolated core region condition and (b) Model II: uniform core temperature condition.

and blood for both tissue/organ models representing isolated and uniform core conditions.

Acknowledgement

The grant from Ohio Supercomputer Center and the use of software is acknowledged and appreciated.

References

[1] S.R.H. Davidson, D.F. James, Drilling in bone: modeling heat generation and temperature distribution, J. Biomech. Eng. 125 (3) (2003) 305–314.

[2] W.G. Sawyer, M.A. Hamilton, B.J. Fregly, S.A. Banks, Temperature modeling in a total knee joint replacement using patient-specific kinematics, Tribol. Lett. 15 (4) (2003) 343–351.

[3] K.J. Chua, J.C. Ho, S.K. Chou, M.R. Islam, On the study of the temperature distribution within a human eye subjected to a laser source, Int. Commun. Heat Mass Transfer 32 (8) (2005) 1057–1065.

[4] J.A. Scott, The computation of temperature rises in the human eye induced by infrared radiation, Phys. Med. Biol. 33 (2) (1988) 243–257.

[5] E.H. Amara, Numerical investigations on thermal effects of laser-ocular media interaction, Int. J. Heat Mass Transfer 38 (13) (1995) 2479–2488.

[6] E.J. Hall, L. Roizin-Towle, Biological effects of heat, Cancer Res. 44 (1984) 4708s–4713s.

[7] S.B. Field, Hyperthermia in the treatment of cancer, Phys. Med. Biol. 32 (7) (1987) 789–811.

[8] M.W. Dewhirst, T.V. Samulski, Hyperthermia in the Treatment for Cancer, Upjohn, Kalamazoo, MI, 1988.

[9] S.B. Field, J.W. Hand, An Introduction to the Practical Aspects of Clinical Hyperthermia, Taylor & Francis, New York, 1990.
[10] P. Wust, B. Hildebrandt, G. Sreenivasa, B. Rau, J. Gellermann, H. Riess, R. Felix, P.M. Schlag, Hyperthermia in combined treatment of cancer, Lancet Oncol. 3 (8) (2002) 487–497.
[11] C.C. Vernon, J.W. Hand, S.B. Field, D. Machin, J.B. Whaley, J. Zee, W.L.J. Putten, G.C. Rhoon, J.D.P. Dijk, D.G. Gonzalez, F.F. Liu, P. Goodman, M. Sherar, Radiotherapy with or without hyperthermia in the treatment of superficial localized breast cancer: results from five randomized controlled trials, Int. J. Radiat. Oncol. Biol. Phys. 35 (4) (1996) 731–744.
[12] J. Zee, D. Gonzalez, G. Rhoon, J. Dijk, W. Putten, A. Hart, Comparison of radiotherapy alone with radiotherapy plus hyperthermia in locally advanced pelvic tumours: a prospective, randomised, multicentre trial, Lancet 355 (9210) (2000) 1119–1125.
[13] B. Rau, P. Wust, P. Hohenberger, J. Loffel, M. Hunerbein, C. Below, J. Gellermann, A. Speidel, T. Vogl, H. Riess, R. Felix, P.M. Schlag, Preoperative hyperthermia combined with radio-chemotherapy in locally advanced rectal cancer: a phase II clinical trial, Ann. Surg. 227 (3) (1998) 380–389.
[14] M. van Vulpen, A.A.C. de Leeuw, B.W. Raaymakers, R.J.A. van Moorselaar, P. Hofman, J.J.W. Lagendijk, J.J. Battermann, Radiotherapy and hyperthermia in the treatment of patients with locally advanced prostate cancer: preliminary results, BJU Int. 93 (1) (2004) 36–41.
[15] D.M. Brizel, R.K. Dodge, R.W. Clough, M.W. Dewhirst, Oxygenation of head and neck cancer: changes during radiotherapy and impact on treatment outcome, Radiother. Oncol. 53 (2) (1999) 113–117.
[16] H.H. Pennes, Analysis of tissue and arterial blood temperature in the resting human forearm, J. Appl. Physiol. 1 (1948) 93–122.
[17] C.K. Charny, Mathematical models of bioheat transfer, Adv. Heat Transfer 22 (1992) 19–155.
[18] H. Arkin, L.X. Xu, K.R. Holmes, Recent developments in modeling heat transfer in blood perfused tissues, IEEE Trans. Biomed. Eng. 41 (1994) 97–107.
[19] W. Wulff, The energy conservation equation for living tissue, IEEE Trans. Biomed. Eng. 21 (6) (1974) 494–495.
[20] H.G. Klinger, Heat transfer in perfused biological tissue. I: General theory, Bull. Math. Biol. 36 (4) (1974) 403–415.
[21] M.M. Chen, K.R. Holmes, Microvascular contributions in tissue heat transfer, Ann. N. Y. Acad. Sci. 335 (1980) 137–150.
[22] Z.S. Deng, J. Liu, Analytical study on bioheat transfer problems with spatial or transient heating on skin surface or inside biological bodies, ASME J. Biomech. Eng. 124 (6) (2002) 638–649.
[23] H. Zhang, Lattice Boltzmann method for solving the bioheat equation, Phys. Med. Biol. 53 (3) (2008) 15–23.
[24] J.W.D. Jrt, P.P. Antich, C.E. Lee, Exact solutions to the multiregion time-dependent bioheat equation. I: Solution development, Phys. Med. Biol. 35 (7) (1990) 847–867.
[25] H.G. Bagaria, D.T. Johnson, Transient solution to the bioheat equation and optimization for magnetic fluid hyperthermia treatment, Int. J. Hyperthermia 21 (1) (2005) 57–75.
[26] L. Zhu, C. Diao, Theoretical simulation of temperature distribution in the brain during mild hypothermia treatment for brain injury, Med. Biol. Eng. Comput. 39 (6) (2001) 681–687.
[27] S. Weinbaum, L.M. Jiji, D.E. Lemons, Theory and experiment for the effect of vascular microstructure on surface tissue heat transfer. Part I: Anatomical foundation and model conceptualization, ASME J. Biomech. Eng. 106 (4) (1984) 321–330.
[28] L.M. Jiji, S. Weinbaum, D.E. Lemons, Theory and experiment for the effect of vascular microstructure on surface tissue heat transfer. Part II: Model formulation and solution, J. Biomech. Eng. 106 (4) (1984) 331–341.
[29] S. Weinbaum, L.M. Jiji, A two phase theory for the influence of circulation on the heat transfer in square tissue, in: M.K. Wells (Ed.), Advances in Bioengineering, New York, 1979, pp. 179–182.
[30] S. Weinbaum, L.M. Jiji, A new simplified bioheat equation for the effect of blood flow on local average tissue temperature, J. Biomech. Eng. 107 (2) (1985) 131–139.
[31] J.W. Mitchell, G.E. Myers, An analytical model of the countercurrent heat exchange phenomena, Biophys. J. 8 (1968) 897–911.
[32] K.H. Keller, L. Seilder, An analysis of peripheral heat transfer in man, J. Appl. Physiol. 30 (5) (1971) 779–789.
[33] P.F. Scholander, J. Krog, Countercurrent heat exchange and vascular bundles in sloths, J. Appl. Physiol. 10 (1957) 405–411.
[34] C. Chen, L.X. Xu, A vascular model for heat transfer in an isolated pig kidney during water bath heating, ASME J. Heat Transfer 125 (5) (2003) 936–943.
[35] Y. Xuan, W. Roetzel, Bioheat equation of the human thermal system, Chem. Eng. Technol. 20 (4) (1997) 268–276.
[36] W. Roetzel, Y. Xuan, Transient response of the human limb to an external stimulus, Int. J. Heat Mass Transfer 41 (1) (1998) 229–239.
[37] A.R. Khaled, K. Vafai, The role of porous media in modeling flow and heat transfer in biological tissues, Int. J. Heat Mass Transfer 46 (2003) 4989–5003.
[38] A. Nakayama, F. Kuwahara, A general bioheat transfer model based on the theory of porous media, Int. J. Heat Mass Transfer 51 (11–12) (2008) 2637–3256.
[39] K. Khanafer, K. Vafai, Synthesis of mathematical models representing bioheat transport, in: W.J. Minkowycz, E.M. Sparrow (Eds.), Advance in Numerical Heat Transfer, vol. 3, Taylor & Francis, 2009.
[40] K. Khanafer, K. Vafai, The role of porous media in biomedical engineering as related to magnetic resonance imaging and drug delivery, Heat Mass Transfer 42 (2006) 939–953.
[41] K. Vafai, C.L. Tien, Boundary and inertia effects on flow and heat transfer in porous media, Int. J. Heat Mass Transfer 24 (1981) 195–203.
[42] M. Sozen, K. Vafai, Analysis of the non-thermal equilibrium condensing flow of a gas through a packed bed, Int. J. Heat Mass Transfer 33 (1990) 1247–1261.
[43] K. Vafai, M. Sozen, Analysis of energy and momentum transport for fluid flow through a porous bed, ASME J. Heat Transfer 112 (1990) 690–699.
[44] M. Quintard, S. Whitaker, Theoretical analysis of transport in porous media, in: K. Vafai (Ed.), Handbook of Porous Media, Marcel Dekker, Inc., New York, 2000, pp. 1–52.
[45] D.Y. Lee, K. Vafai, Analytical characterization and conceptual assessment of solid and fluid temperature differentials in porous media, Int. J. Heat Mass Transfer 42 (1999) 423–435.
[46] A. Amiri, K. Vafai, Analysis of dispersion effects and nonthermal equilibrium, non-Darcian, variable porosity incompressible flow through porous medium, Int. J. Heat Mass Transfer 37 (1994) 939–954.
[47] B. Alazmi, K. Vafai, Constant wall heat flux boundary conditions in porous media under local thermal non-equilibrium conditions, Int. J. Heat Mass Transfer 45 (2002) 3071–3087.
[48] A. Amiri, K. Vafai, T.M. Kuzay, Effect of boundary conditions on non-Darcian heat transfer through porous media and experimental comparisons, Numer. Heat Transfer A 27 (1995) 651–664.
[49] A. Marafie, K. Vafai, Analysis of non-Darcian effects on temperature differentials in porous media, Int. J. Heat Mass Transfer 44 (2001) 4401–4411.
[50] D.A. Nield, A. Bejan, Convection in Porous Media, third ed., Springer, New York, 2006. pp. 27–38.
[51] J.C. Chato, Heat transfer to blood vessels, ASME J. Biomech. Eng. 102 (2) (1980) 110–118.
[52] S. Mahjoob, K. Vafai, Analytical characterization and production of an isothermal surface for biological and electronics applications, ASME J. Heat Transfer, in press.
[53] FLUENT 6.3 Users's Guide, 2006, Lebanon, US.
[54] S.V. Patankar, Numerical Heat Transfer and Fluid Flow, McGraw-Hill, New York, 1980.